

Spring bloom onset in the Nordic Seas

A. Mignot^{1*}, R. Ferrari¹, and K. A. Mork^{2,3}

¹ Massachusetts Institute of Technology, Cambridge, MA, USA.

² Institute of Marine Research, Bergen, Norway.

³ Bjerknes Centre for Climate Research, Bergen, Norway.

*Corresponding author: mignot@mit.edu.

Abstract

The North Atlantic spring bloom is a massive annual growth event of marine phytoplankton, tiny free-floating algae that form the base of the ocean's food web and generates a large fraction of the global primary production of organic matter. The conditions that trigger the onset of the spring bloom in the Nordic Seas, at the northern edge of the North Atlantic, are studied using in-situ data from six bio-optical floats released above the Arctic Circle. It is often assumed that spring blooms start as soon as phytoplankton cells daily irradiance is sufficiently abundant that division rates exceed losses. The bio-optical float data instead suggest the tantalizing hypothesis that Nordic Seas blooms start when the photoperiod, the number of daily light hours experienced by phytoplankton, exceeds a critical value, independently of division rates. The photoperiod trigger may have developed at high latitudes where photosynthesis is impossible during polar nights and phytoplankton enters in a dormant stage in winter. While the first accumulation of biomass recorded by the bio-optical floats is consistent with the photoperiod hypothesis, it is

1 possible that some biomass accumulation started before the critical photoperiod but at levels too
2 low to be detected by the fluorometers. Thus more precise observations are needed to test the
3 photoperiod hypothesis.

4

5 **1. Introduction**

6 The Nordic Seas (Norwegian, Greenland, and Iceland Seas) experience some of the largest
7 carbon dioxide (CO₂) fluxes anywhere in the ocean resulting in a carbon uptake of 20-85 g C m⁻²
8 yr⁻¹ (Takahashi et al., 2002). In the Greenland Sea it has been estimated that one third of the
9 annual carbon uptake is driven by export production from biological activity, while the rest is the
10 result of CO₂ dissolution in cold waters that sink into the abyss (Skjelvan et al., 2005). Most of
11 the biological production occurs during ephemeral spring blooms lasting only a few weeks. A
12 good understanding of the conditions that trigger these blooms is thus a prerequisite to quantify
13 and model the carbon budget of the Nordic Seas.

14 In winter, phytoplankton populations decay because losses from respiration, grazing, and
15 viral infections exceed growth. Blooms develop in spring when division rates increase and/or
16 loss rates decrease. Phytoplankton division rates increase with abundance of nutrients and light.
17 At high latitudes, nutrients are plentiful in winter, because the strong upper ocean mixing
18 generated by winds and cooling brings deep nutrients to the surface. Thus light appears to be the
19 limiting factor for winter growth in the sub-polar gyres, as argued in the seminal works of Gran
20 and Braarud (1935), Riley (1946) and Sverdrup (1953). However, it was soon noted that the
21 surface light levels in winter are sufficient for photosynthesis growth even at these latitudes.

1 Thus, the light limitation has been attributed to mixing that keeps phytoplankton cells away from
2 the well-lit surface for long periods of time. Sverdrup (1953) formalized this view and suggested
3 that blooms develop when mixing weakens at the end of winter and phytoplankton spend more
4 time close to the surface to receive enough light to grow in spite of losses. More recently,
5 Behrenfeld and colleagues (2013, 2014) pointed out that blooms can alternatively develop when
6 a disturbance in the predator-prey balance reduces the loss rates below the division rates. The
7 disturbance may be initiated by winter mixing that dilutes both phytoplankton and herbivores
8 reducing their encounter rate and hence the grazing rates (Behrenfeld, 2010). It may also be
9 triggered by an improvement in growth conditions, such light exposure or nutrient availability
10 that causes the division rates to accelerate and to outcompete the grazing rates.

11 These ideas dominate thinking about bloom dynamics, but they may not be as relevant to
12 understand blooms in the Nordic Seas. At these extreme latitudes, insolation drops dramatically
13 in winter. North of the Arctic Circle, no light is received at the ocean surface during polar nights.
14 Phytoplankton growth is simply impossible for days to weeks, depending on the latitude,
15 regardless of mixing levels. It is therefore natural to ask how do phytoplankton populations
16 survive such harsh conditions and what triggers their resurgence in spring.

17 In this manuscript, we study the development of blooms in the Nordic Seas using in-situ
18 profiles of phytoplankton from six bio-optical floats released north of the Arctic Circle. The
19 floats were instrumented with miniaturized bio-optical sensors, which measure chlorophyll
20 concentrations in the upper kilometer of the ocean for one to two years. The data suggest that at
21 these high latitudes, one of two possible scenarios explains the onset of the Nordic Seas blooms
22 observed by the floats: the critical photoperiod hypothesis or the critical depth hypothesis.

1 The paper is organized as follows. We introduce the datasets used in the study in Section 2.
2 Section 3 provides a preliminary analysis of the data with the conclusion that two possible
3 interpretations can explain the onset of the Nordic Seas blooms. In Section 4, we develop the
4 theoretical framework to test the two hypotheses. This framework is then used in Section 5.
5 Finally, Section 6 summarizes and discusses the results.

6

7 **2. Data**

8 **a. Floats deployed north of the Arctic Circle**

9 Our results are based on measurements collected with six bio-optical profiling floats deployed in
10 the Nordic Seas, by the Institute of Marine Research in Norway (see Figure 1 and Table 1).
11 Three floats were deployed in 2010 (IMR1, IMR2 and IMR3) and three floats were deployed in
12 2014 (IMR4, IMR5, and IMR6). The float data were downloaded from the Coriolis data center
13 (<http://www.coriolis.eu.org/>). The three floats deployed in 2010 were in the water for two years
14 and returned observations of six spring blooms. The three floats deployed in 2014 are still
15 operating and sampled the 2014-2015 spring bloom.

16 We consider measurements made by the floats IMR1, IMR2 and IMR3 from September
17 2010 to June 2011 and from September 2011 to June 2012, time periods long enough to capture
18 the onset of the spring blooms—the float IMR3 was deployed in November 2010 and hence the
19 analysis start in November of that year. Measurements from floats IMR4, IMR5 and IMR6 span
20 the interval from September 2014 to June 2015.

21 **b. Float deployed South of the Arctic Circle**

1 Two bio-optical floats (IMR7 and IMR8), deployed in November 2013 and July 2014
2 respectively, observed a spring bloom south of the Arctic Circle. These floats are used to
3 compare blooms north and south of Arctic Circle and better illustrate the effect of complete
4 darkness on the phytoplankton dynamics. The IMR7 and IMR8 float data were also downloaded
5 from the Coriolis data center.

6 **c. Floats instrumentation and calibration**

7 All floats were APEX float profilers, equipped with a WET Labs ECO FLNTU
8 comprising a chlorophyll fluorometer, and a backscattering sensor at 700 nm. The IMR1-3 and
9 IMR7 floats included a SEABIRD dissolved oxygen sensor while the IMR4-6 and IMR8 floats
10 included an Aanderaa optode [O₂] sensor.

11 The IMR1-3 floats nominal mission included CTD and optical profiles from 1000 m to
12 the surface. The sampling resolution was 25 m from 1000 m to 350 m, 10m from 350m to 100m,
13 and 5 m from 100m to the surface. The IMR4-8 floats nominal mission included CTD and
14 optical profiles from 2000 m to the surface. The sampling resolution was 50 m from 2000 m to
15 1000 m, 20 m from 1000 m to 500 m, 10 m from 500 m to 200 m, and 5 m from 200m to the
16 surface. The upward casts were repeated every 5 or 10 days. The floats typically emerged from
17 the sea around midnight, but, occasionally, they reached the surface in the morning or in the
18 afternoon.

19 The CTD data were quality-controlled using the standard Argo protocol (Wong et al.,
20 2010). The fluorescence raw signals (counts) were transformed into Chl *a* concentration, [Chl *a*],
21 expressed in mg m⁻³ via a scale factor and after the nominal instrument-specific dark counts had
22 been subtracted. The manufacturer provides two parameters for converting measured

1 fluorescence counts to estimated [Chl *a*]: a nominal instrument-specific dark counts and a scale
2 factor expressed in mg m⁻³ relating measured fluorescence minus the dark counts to [Chl *a*].

3 We tested the accuracy of the scale factor provided by the manufacturer against a slope
4 determined by a regression between the float fluorescence (minus the dark counts) and [Chl *a*]
5 estimates from Moderate Resolution Imaging Spectroradiometer (MODIS)—a method first
6 proposed by Boss et al. (2008). The satellite [Chl *a*] estimates represent a measurement
7 weighted from the surface to the depth at which the light intensity is 1% of its surface value. For
8 comparison with MODIS data, float fluorescence measurements were therefore weighted in the
9 same way; i.e :

$$fl_{surf} = \frac{\sum e^{-2K_d(490)z} fl(z)}{\sum e^{-2K_d(490)z}}, \quad (1)$$

10 where $fl(z)$ is the vertical profile of fluorescence minus the dark counts, and $K_d(490)$ is the
11 diffuse attenuation coefficient for downwelling irradiance at 490 nm estimated by MODIS.
12 We used the 8-day level 3 MODIS composites in 1°×1° boxes centered on the float locations for
13 match up data. The MODIS matchups for all floats were used to estimate the regression slopes.
14 These regression coefficients were significantly smaller than those provided by the
15 manufacturer's for our fluorometers (see Table 2). The variations in regression slopes from
16 MODIS are likely due to uncertainties in the matchups: we are regressing 1°×1° satellite data to
17 pointwise measurements. Thus, we computed the MODIS-based correction by averaging over all
18 eight floats and applied a 0.0029 +/- 0.0014 mg m⁻³ count⁻¹ slope to compute chlorophyll from
19 the eight fluorometers. Applying individual regression slope results in very different chlorophyll
20 values for each float despite the fact that the floats sampled the same general region.

1 The winter backscatter values in the mixed layer were always lower than the values below;
2 possibly because particles below the mixed layer have different composition than those above.
3 Regardless, this prevents us to use these data to investigate the phytoplankton dynamics.

4 **a. Atmospheric and solar variables**

5 In our analysis, we need estimates of the heat and freshwater fluxes that drive upper
6 ocean turbulence and the photosynthetically active radiation (PAR). The hourly net atmospheric
7 heat fluxes (Q_0 in $W m^{-2}$) were taken from the ECMWF ERA-interim reanalysis (Dee et al.,
8 2011). We ignored the freshwater fluxes that are a minor contributor to upper ocean turbulence
9 in the winter North Atlantic (Ferrari et al., 2014). Time series of the heat fluxes along the float
10 trajectories were then generated by averaging the daily ERA-interim values in one by one degree
11 bins around the float daily positions.

12 The clear sky instantaneous PAR in $\mu mol photons m^{-2} s^{-1}$, $iPAR(0,t)_{clear}$, was calculated using
13 the Gregg and Carder (1990) solar irradiance model for a free-cloud sky. The reduction of the
14 photosynthetically active radiation due to clouds was estimated with the formulation of Budyko
15 et al. (1964):

$$iPAR(0, t) = iPAR(0, t)_{clear}(1 - 0.14c - 0.38c^2) \quad (2)$$

16 where c is the total cloud cover. The total cloud cover c , varying from 1 for an overcast sky to 0
17 for a clear sky, was taken from ECMWF ERA-interim reanalysis averaged along the float
18 trajectories as described for the heat fluxes. The daily averaged sea surface PAR in $mol photons$
19 $m^{-2} day^{-1}$, $PAR(0)$, was obtained by averaging Eq. (2) over the length of the day.

1 Finally, to test the photoperiod hypothesis we need estimates of the length of daytime.
2 The length of daytime (dl in hours) was calculated with the package geosphere from the R
3 software (R Development Core Team, 2016), which computes the length of the daytime for a flat
4 surface for a given latitude and day of year (Forsythe et al., 1995).

5 **b. Float estimates of mixed layer and euphotic layer depth**

6 In the analysis to follow, we need estimates of the mixed layer depth, the layer where
7 density is well homogenized (as a layer where mixing is active), and the euphotic layer depth, the
8 depth below which the light level is too low to support photosynthesis.

9 For all floats but one, the mixed layer depth (H) was computed as the depth at which the
10 density change from its value at 10 m is $\Delta\sigma_\theta = 0.01 \text{ kg m}^{-3}$ (Kara et al. (2000, 2003)). We chose
11 the value of $\Delta\sigma_\theta$ that best tracked the region of weak stratification in our dataset. This value is
12 consistent with the study of Brainerd and Gregg (1995) who also found that a $\Delta\sigma_\theta$ of 0.005- 0.01
13 kg m^{-3} often marks the base of the active turbulent surface layer. The salinity sensor was
14 defective in the float IMR2 and H was computed as the depth at which the temperature change
15 from its value at 10 m is $\Delta\theta = 0.15 \text{ }^\circ\text{C}$, which corresponds to $\Delta\sigma_\theta \sim 0.01 \text{ kg m}^{-3}$ for a salinity of
16 35.2 representative of values observed in the Nordic Seas.

17 The surface value of [Chl *a*] ($[\text{Chl}]_{\text{ml}}$, mg m^{-3}) was calculated as the average within the
18 mixed layer (ML). The vertical integral of [Chl *a*] ($\langle \text{Chl} \rangle$, mg m^{-2}) was obtained by integrating
19 the vertical profile of [Chl *a*] from the surface down to the ML base.

20 We defined the instantaneous euphotic layer depth $iH_{\text{eu}}(t)$ as the depth below which the
21 light level is too low to support photosynthesis. The threshold light level was set to $1 \text{ } \mu\text{mol}$
22 $\text{quanta m}^{-2} \text{ s}^{-1}$, corresponding to the lowest light levels at which the temperate diatom

1 *Phaeodactylum-tricornutum* has been observed to grow (Geider et al., 1986). Following the
 2 Beer-Lambert law, the incoming solar radiation was assumed to decay exponentially with depth.
 3 The decay rate, equal to the inverse of the diffuse coefficient attenuation of light K (m^{-1}), was set
 4 to a constant value with depth and throughout the day. Therefore, K was given by:

$$K = \frac{\log(0.01)}{H_{1\%}}. \quad (3)$$

5 The depth $H_{1\%}$ at which the light intensity is 1% of its surface value was calculated from $[Chl]_{ml}$
 6 using the empirical relationship derived by (Morel et al., 2007) from a global datasets of ship-
 7 based measurements of $H_{1\%}$ and surface $[Chl a]$:

$$\begin{aligned} \log_{10} H_{1\%} = & \quad (4) \\ & = 1.524 - 0.436 \times \log_{10} [Chl]_{ml} - 0.0145 \times (\log_{10} [Chl]_{ml})^2 + 0.0186 \times \\ & (\log_{10} [Chl]_{ml})^3. \end{aligned}$$

9 Whenever K was estimated to be lower than the diffuse coefficient attenuation of light by pure
 10 water $K_w = 0.027 m^{-1}$ (Smith and Baker, 1981), K was set to K_w .

11 Then, $iH_{eu}(t)$ was estimated as the depth where the irradiance is $1 \mu mol \text{ quanta } m^{-2} s^{-1}$:

$$iH_{eu}(t) = \frac{1}{K} \log \left(\frac{iPAR(0, t)}{1} \right), \quad (5)$$

12 where $iPAR(0, t)$ is the clear sky instantaneous PAR. Finally, we found that $iHeu(t)$ transitions
 13 vary rapidly from zero at night to its maximum value during the day, so that it can be described
 14 by a rectangle function which transitions abruptly from zero at night to the value given by Eq.

1 (5). The height of the function is the daily-averaged euphotic layer, H_{eu} (m), for the whole
2 duration of the day.

3 **3. Data Analysis**

4 From fall to spring, in each of the nine blooms sampled by the floats north of the Arctic
5 Circle (two years each from IMR1, IMR2, IMR3 and one year from IMR4, IMR5 and IMR6), we
6 observed the same qualitative pattern in the evolution of the ML depth and the Chl a
7 concentration. Figure 2 shows as an example the potential density anomaly (σ_θ), and [Chl a],
8 acquired by the float IMR2 from September 2011 to June 2012. (Figures for the other eight years
9 are displayed in the supplementary material Figs. S1-S9.) The ML and euphotic depths are
10 marked as continuous and dashed black lines respectively. Figure 2a shows that in fall, from
11 September to December, the [Chl a] decreased and the ML deepened. The fluorescence signal
12 dropped to its minimum value from late December-early January during the polar night and the
13 values were essentially uniform from the ML down to 1000 m (not shown) for the following
14 several weeks.

15 To test whether the polar night ML [Chl a] was too low to be detected by the fluorometer,
16 we compared the fluorescence measurements collected in the ML, where one expects to find
17 some low [Chl a], with those collected between 900 m and 1000 m, where no [Chl a] is expected
18 and the fluorescence values can be used as an estimate of the dark signal, i.e. fluorescence values
19 measured in the absence of [Chl a]. For each profile collected from December to April, we
20 checked whether the distribution of fluorescence values in the ML was significantly different
21 from the distribution of values between 900 and 1000 m using a two-sample Mann-Whitney-
22 Wilcoxon test. The Mann-Whitney-Wilcoxon test confirmed that during winter, the ML

1 fluorescence values were not different from the deep values at the 95% confidence level (marked
2 with an asterisk in the figures). In other words, the winter [Chl a] in the ML was on average too
3 low to be detected by the fluorometer. However, the fluorometers detected numerous spikes of
4 higher than average [Chl a] in the winter ML, but not at depth. This suggests that the winter [Chl
5 a] was just below detection levels in winter and occasionally the signal emerged above the noise.
6 Similar results were obtained for all others floats deployed north of the Arctic Circle.

7 The winter [Chl a] profiles from floats IMR7 and IMR8, which profiled south of Arctic
8 Circle in winter, were very different from those north of the Arctic Circle as shown in Figs. 3 and
9 S11. These profiles were characterized by ML fluorescence values significantly higher than
10 those at deeper depths even in winter; most likely because the [Chl a] remained high enough to
11 be detected by the fluorometer. This last point is important, because it suggests that a period of
12 complete darkness depletes the phytoplankton biomass so dramatically that most of the time
13 traditional fluorometers cannot detect its concentration.

14 The ML fluorescence values north of the Arctic Circle emerged from the fluorometer
15 noise level after the end of the polar night. The time of “emergence from noise” t_E , was defined
16 as the first instance (second white vertical line in Fig. 2), when the ML fluorescence values
17 became significantly greater than the deep fluorescence values as per the Mann-Whitney-
18 Wilcoxon test in three consecutive profiles (~ 1 month). The positions of the floats at t_E for all
19 floats deployed north of the Arctic Circle are shown as black dots in Fig. 1.

20 The net accumulation of [Chl a] starting at t_E was detected both in surface $[Chl]_{ml}$ and
21 vertically integrated $\langle Chl \rangle$, and lasted until June-July. We cannot determine whether
22 accumulation started at t_E or earlier, when the fluorescence values were too low to be detected by

1 the fluorometer. Given that photoautotrophic growth is not possible without light, we can
2 however conclude that the bloom must have started sometime between the end of the polar night
3 and t_E . We will refer to this time interval as Δt_{onset} (shown as a gray shading area in Fig. 2).

4 Figure 4 shows the surface heat fluxes, the ML depth, the daily averaged PAR and the
5 length of daytime with time shifted so that the origin is at $t = t_E$ for each of the nine float years.
6 The time of “emergence from noise” for seven out of nine events (blue lines) occurred when the
7 daylength was between 9 and 11 hours (Fig. 4d) and $\text{PAR}(0)$ was between 3 and 8 mol quanta m^{-2}
8 day^{-1} (Fig. 4c). The surface heat flux Q_0 was moderately negative, between 100 and 200 W m^{-2}
9 (Fig. 4a), and the ML was as likely to be shoaling or deepening (Fig. 4b). Table 3 shows that t_E
10 occurred between year-day 59 and 72 for all years. Moreover, t_E occurred earlier for the floats
11 that were further south. For the two other events (red lines), Figs 4a and 4b show that the time of
12 “emergence from noise” coincided with the shutdown of convection and the sudden shoaling of
13 the ML, when the daylength was approximately 14 hours, $\text{PAR}(0)$ was ~ 12 mol quanta $\text{m}^{-2} \text{day}^{-1}$
14 and the day of the year was between 95 and 96 (Table 2).

15 Two possible bloom onset scenarios emerge from this simple preliminary analysis of the
16 float data. One interpretation is that blooms started at $t = t_E$, when the accumulation of
17 phytoplankton biomass was first detected by the fluorometer, and the photoperiod (the duration
18 of a phytoplankton cell daily exposure to light) reached a critical value of 10 ± 1 hours. For the
19 seven events with shallow MLs, the photoperiod was equal to the daylength (see Fig. 5). In the
20 two cases with deep MLs, the phytoplankton did not experience 10 ± 1 hours of light until the
21 mixing subsided and allowed cells to linger at the surface—this is shown more quantitatively in
22 the next section. This interpretation is supported by two lines of evidence. First, it is statistically
23 very unlikely that the co-occurrence of a particular daylength and the first increase in

1 chlorophyll detected by all fluorometers is mere coincidence, as would have to be argued
2 if t_E represented the emergence of fluorescence signal from background noise. Second, the
3 repeated detection of significant fluorescent spikes in the winter ML profiles suggests that the
4 winter $[Chl]_{ml}$ was just below detection levels and thus the emergence from noise was likely
5 close to the actual increase in chlorophyll. (We focus our discussion on photoperiod, because
6 attempts to correlate the bloom onset with daily averaged light or maximum iPAR did not
7 collapse the data as well due to large cloud coverage variations from year to year.)

8 A second interpretation is that all bloom onsets are consistent with the critical depth
9 hypothesis. Blooms started when phytoplankton division rate became larger than the
10 phytoplankton loss rates. However, the biomass accumulation was so weak during Δt_{onset} that
11 went undetected by the fluorometers. In this interpretation, the coincidence of the emergence of
12 the fluorescence signal from noise and the photoperiod must be considered a statistical fluke. We
13 develop the theoretical framework to test these two possible scenarios in the next section.

14

15 **4. Theory**

16 **a. Critical photoperiod hypothesis**

17 In the Nordic Seas, the insolation drops dramatically in winter. As one moves north of the
18 Arctic Circle, there are progressively longer periods of complete winter darkness, the polar
19 nights. Phytoplankton growth is simply impossible for days to weeks, depending on the latitude.
20 Under these conditions, the focus must shift on understanding how phytoplankton cells survive
21 the winter darkness to give rise to a bloom in spring. With no energy to photosynthesize, cells

1 will likely strive to reduce losses due to metabolic respiration, grazing pressure, parasitism, and
2 viral infections. We review recent literature suggesting that the cells enter in a dormant state
3 during polar nights and then wake up, when the daylength crosses some threshold.

4 Eilertsen (1995) studied the onset of spring blooms in the coastal waters of the Nordic
5 Seas. While coastal blooms may be different from open ocean blooms – the focus of our study –
6 some key findings are worth reviewing. These blooms are dominated by marine diatoms in the
7 early stages and begin approximately the same calendar day every year, despite highly variable
8 year-to-year environmental conditions. Field studies showed that in the coastal waters of
9 Northern Norway, the marine diatoms turn into resting spores during winter to drastically reduce
10 respiration and survive several weeks of darkness (Degerlund and Eilertsen, 2010). The heavy
11 spores sink to the bottom a few hundred meters below the surface into permanent darkness.
12 However, they are occasionally re-suspended towards the surface by sudden mixing events
13 triggered by atmospheric storms. Eilertsen et al. (1995) speculated that the spores germinate
14 when the daylength exceeds a critical threshold; estimated between 7 and 12 h (Eilertsen and
15 Wyatt, 2000). Note that this survival strategy is not specific to diatoms. Many species of
16 dinoflagellates and chrysophytes produce cysts at the end of summer or in response to
17 environmental stimuli, such as nutrient limitation, and remain dormant until the following spring.
18 Some are known to germinate in response to light or nutrient stimulation. Others germinate after
19 a specific period of time or in response to photoperiod (McMinn and Martin, 2013).

20 A daylength control has never been documented in the open ocean of the Nordic Seas,
21 possibly due to the dearth of ocean color measurements in winter when cloud coverage is
22 ubiquitous. Moreover, in the open ocean the hypothesis must be modified because the

1 photoperiod can be shorter than the daylength, when strong mixing keeps cells below the
2 euphotic layer for some part of the daytime as shown in Fig. 4.

3 It has been documented that plant systems determine the photoperiod by sensing the
4 duration of darkness (Hamner, 1940; Hamner and Bonner, 1938). In an ocean environment
5 photoperiod based on “darkness-length” is not a viable strategy: the length of darkness correlates
6 primarily with the strength of mixing, which keeps cells away from the surface, and not with the
7 number of light hours at the surface. If cells relied on sampling the number of dark hours, they
8 would germinate every time a strong storm passed by, suddenly deepening the mixed layer and
9 increasing the number of hours without light they experienced. Therefore, photoperiod in the
10 ocean must be based on the length of “light-hours”, if it is to be a viable strategy. We are not
11 aware of studies that investigated how phytoplankton detect photoperiod, but our results suggest
12 that it would be an interesting area of research.

13 In the appendix, we derive an approximate formula to calculate the photoperiod in the open
14 ocean as a function of daylength, euphotic layer depth and strength of mixing. In section 5, we
15 will confirm that the first accumulation of chlorophyll detected by the fluorometers occurred at
16 the same critical photoperiod, supporting the hypothesis that the onset of the Nordic Seas blooms
17 is consistent with a critical photoperiod hypothesis.

18 **b. Critical depth hypothesis**

19 Following Sverdrup (1953), the changes in phytoplankton concentration $P(z, t)$ in response
20 to changes in light, grazing and vertical mixing can be described by a partial differential
21 equation:

1

$$\frac{\partial P(z, t)}{\partial t} = \mu(z, t)P(z, t) - m(z, t)P(z, t) + \frac{\partial}{\partial z} \left(\kappa_T(z, t) \frac{\partial P(z, t)}{\partial z} \right), \quad (6)$$

2 where z is the vertical coordinate, t is time, μ is the cell division rate, m is the phytoplankton loss
 3 rate and κ_T is the vertical eddy diffusivity, which represents the rate at which turbulence mixes
 4 phytoplankton in the vertical. The effect of light on growth is captured by the depth and time
 5 dependence of the division rate. Nutrient limitation on growth is ignored, because in the early
 6 phase of blooms in the Nordic Seas nutrients are plentiful. Finally, we ignore the effect of lateral
 7 advection of phytoplankton by oceanic currents. This is a reasonable assumption as long as the
 8 currents are weak or the phytoplankton concentrations are uniform in the horizontal. We cannot
 9 test whether this is always the case for the float data, so we will use this equation as a working
 10 hypothesis and check to what extent the terms included in the right hand side are sufficient to
 11 explain the observed changes in $P(z, t)$.

12 When turbulence is strong, like in the Nordic Seas winter, the phytoplankton is mixed so fast
 13 that it remains uniform within the ML and we can ignore the z dependence in P . We also assume
 14 assuming that there is no phytoplankton flux through the surface and the ML base. Integrating
 15 Eq. (6) over the mixed layer in addition to averaging over a full day (indicating by an overbar),
 16 we obtain an expression for the phytoplankton growth rate:

17

$$\int_{-H}^0 \frac{\partial \bar{P}}{\partial t} dz = \langle \bar{\mu} \rangle \bar{P} - \langle \bar{m} \rangle \bar{P}, \quad (7)$$

1 where $\langle \rangle$ represents the vertical integral between the surface and the ML base at $z=-H$. The total
2 population size can grow when the left-hand side is positive, or

3

$$\langle \bar{\mu} \rangle \geq \langle \bar{m} \rangle. \quad (8)$$

4 If following Sverdrup (1953), we further assume that the losses are independent of depth, since
5 they depend on phytoplankton and zooplankton concentrations which are uniform with depth,
6 then $\langle \bar{m} \rangle = H\bar{m}$, and accumulation occurs if the mixed layer depth is shallower than a critical
7 depth

$$H \leq H_c = \frac{\langle \bar{\mu} \rangle}{\bar{m}}, \quad (9)$$

8 or state differently; when the daily mixed layer averaged division rate is greater than the loss
9 rates:

$$\frac{1}{H} \langle \bar{\mu} \rangle \geq \bar{m}. \quad (10)$$

10 Despite its simplicity, the condition necessary for bloom onset in the limit of strong turbulence is
11 difficult to test quantitatively with profiling float data. Testing Eq. (10) requires in situ
12 observations of phytoplankton division and loss rates, which presently cannot be measured with
13 autonomous platforms. Phytoplankton division rate can however be estimated using bio-optical
14 models. Then, phytoplankton loss rates can then be derived from Eq. (7) by subtracting the net
15 accumulation rate (i.e., $\frac{1}{\bar{P}} \int_{-H}^0 \frac{\partial \bar{P}}{\partial t} dz$) from $\langle \bar{\mu} \rangle$.

1 To avoid any confusion down the road, it is worth emphasizing that the critical depth
 2 framework remains the key approach to study the development of blooms. There is however, an
 3 ongoing discussion as to what are the key variables that change at bloom onset and Eq. (10) to be
 4 first satisfied. Sverdrup (1953) hypothesized that Eq. (10) is typically satisfied at the end of
 5 winter, when the ML depth H shoals resulting in an increase of $\frac{1}{H}\langle\bar{\mu}\rangle$. Behrenfeld and colleagues
 6 (2013; 2014) argued that the left and right hand side terms are always very close to exact
 7 balance. Blooms start whenever a small perturbation in the system drives $\frac{1}{H}\langle\bar{\mu}\rangle$ to increase
 8 above \bar{m} , including late fall conditions when \bar{m} decreases rapidly due to ML deepening and
 9 associated dilution of grazers (Behrenfeld, 2010). Finally, it is also possible for blooms to start in
 10 response to an increase in light, and hence $\langle\bar{\mu}\rangle$, with no changes in the other variables. In the
 11 following, we will use the critical depth framework to interpret the float data, with the goal of
 12 determining what processes first trigger the bloom.

13 **i. Phytoplankton division rates**

14 The division rate μ in Eq. (6) represents the division rate of the overall phytoplankton
 15 population. We used the physiological model of Geider et al. (1997), together with the photo-
 16 physiological parameters from Antoine and Morel (1996), to get an estimate of the division rate.

17 Geider et al. (1997) proposed that the nutrient-saturated division rates are well described
 18 by the equation:

19

$$\mu(z, t) = \mu_{max} \left(1 - e^{-\frac{\alpha_{chl} \times \theta_c \times IPAR(z,t)}{\mu_{max}}} \right), \quad (11)$$

1 where μ_{\max} is the maximum value of the division rate under light-saturated conditions (s^{-1}), α_{chl} is
 2 the Chl a-specific initial slope of the photosynthesis-irradiance curve [$gC\ gChla^{-1}\ (\mu mol\ quanta)^{-1}$
 3 m^2], and θ_c is the chlorophyll to carbon ratio. We verified that in winter light levels are low
 4 enough that Eq. (11) is well approximated by the linearized version:

$$\mu(z, t) \sim \alpha_{chl} \theta_c iPAR(z, t). \quad (12)$$

6 The Chl a-specific initial slope of the photosynthesis-irradiance curve is set to $6.4 \cdot 10^{-6}\ gC$
 7 $gChla^{-1}\ (\mu mol\ quanta)^{-1}\ m^2$, a value used in a global light-photosynthesis model of oceanic
 8 primary production (Antoine and Morel, 1996). The chlorophyll to carbon ratio θ_c is set to 0.045
 9 $gChla\ gC^{-1}$, a value representative of photoacclimation to extreme low light levels (Westberry et
 10 al., 2008).

11 The vertical profile of $iPAR$ ($\mu mol\ photons\ m^{-2}\ s^{-1}$) is modeled through:

$$iPAR(z, t) = iPAR(0, t) e^{Kz}. \quad (13)$$

12 Finally, we are interested in sustained growth rates for at least a day, not transient growth rates
 13 lasting only a few hours. Consistently we averaged Eq. (12) over a full day in addition to
 14 integrating over the full ML depth:

$$\langle \bar{\mu} \rangle \sim - \frac{\alpha_{chl} \theta_c PAR(0) (e^{-KH} - 1)}{KH} \quad (14)$$

16

17 **ii. Phytoplankton loss rates**

1 Phytoplankton loss rates are given by the sum of grazing, viral lysis and parasitism.
 2 These terms are very difficult to estimate in situ. Instead we will estimate the loss rates as the
 3 residual between the division rates, $\langle \bar{\mu} \rangle$, and the phytoplankton accumulation rates averaged over
 4 a day.

5 Assuming that phytoplankton concentration and loss rates are uniform over the ML
 6 depth, we can derive two separate equations to estimate loss rates during time of ML deepening
 7 and shoaling respectively (Behrenfeld et al., 2013). When the mixed layer deepens and entrains
 8 fluid with no phytoplankton from below, Eq. (6) can be vertically integrated and time averaged
 9 over a few days to obtain an equation for the standing stock, $\langle P \rangle = \int_{-H}^0 P(z) dz = HP$,

$$\frac{d\langle \bar{P} \rangle}{dt} = \frac{1}{H} \langle \bar{\mu} \rangle \langle \bar{P} \rangle - \bar{m} \langle \bar{P} \rangle, \quad (15a)$$

10 where we ignored temporal correlations between the daily variations in division rates and the
 11 slower variations in phytoplankton concentrations and grazing rates. Eq. (15a) can now be used
 12 to estimate the vertically integrated and time averaged loss rates,

$$\bar{m} = \frac{1}{H} \langle \bar{\mu} \rangle - \frac{1}{\langle \bar{P} \rangle} \frac{d\langle \bar{P} \rangle}{dt}. \quad (15b)$$

13 During time when the ML shoals and leaves phytoplankton behind, the time and vertical
 14 average of Eq. (6) gives

$$\frac{d\bar{P}}{dt} = \frac{1}{H} \langle \bar{\mu} \rangle \bar{P} - \bar{m} \bar{P}, \quad (16a)$$

15 and

$$\bar{m} = \frac{1}{H} \langle \bar{\mu} \rangle - \frac{1}{\bar{P}} \frac{d\bar{P}}{dt}. \quad (16b)$$

1 Equations (15b) and (16b) are very similar except for the appearance of a standing stock
2 $\langle P \rangle$ versus a concentration P in the right hand side. In section 5, we will estimate the
3 phytoplankton loss rates from Eqs. (15b) or (16b), depending on whether the ML is deepening or
4 shoaling, and use estimates of $\langle \bar{\mu} \rangle$ based on the algorithm given in section 4bi and rates of [Chl
5 a] accumulation from the float data.

6

7 **5. Testing bloom onset hypotheses**

8 Using the theoretical framework that we developed in the last section, we will now test
9 the two bloom onset scenarios that emerged from the preliminary analysis of the float data.

10 **a. Critical photoperiod hypothesis**

11 First, we test whether the start of the Nordic Seas blooms is consistent with the critical
12 photoperiod hypothesis. To do so, we estimate the photoperiod at the time when the fluorometers
13 detected the first accumulation of biomass, i.e., at $t = t_E$. The photoperiod is calculated with the
14 algorithm presented in the appendix. Notice that in this section we therefore assume that the
15 bloom onset coincided with the first increase detected in fluorescence.

16 In Section 3, we anticipated that at $t = t_E$, the daylength was between 9 and 11 hours for the
17 seven years when biomass accumulation was detected with negative sea surface heat fluxes. The
18 formula we developed in the appendix suggests that for these seven blooms the daylength is a
19 pretty accurate estimate of the photoperiod, because the cells remained in the euphotic layer for

1 the whole daylength when the surface heat losses are smaller than 200 W m^{-2} . The onset of these
2 blooms is therefore consistent with a critical photoperiod of 10 ± 1 hours. The daylength
3 increases by one hour every 10 days along the Arctic circle, so the photoperiod cannot be
4 determined to better than one hour with the 10-day float sampling frequency.

5 In the remaining two blooms with winter mixed layers much deeper than 200m, the
6 fluorometers detected the first biomass accumulation when the heat losses and hence mixing
7 subsided at the end of winter. In the weeks preceding $t = t_E$, when the daylength was between 9
8 and 14 hours, the heat losses were constantly above 200 W m^{-2} (Fig. 4a). In the appendix, we
9 show that the strong heat losses generated such intense mixing that the cells never experienced
10 more than 8 hours of light. Hence, the photoperiod experienced by the cells did not reach the 10
11 hours threshold until the cooling finally subsided at the end of March. Therefore, the onset of
12 these two late blooms is also consistent with a critical photoperiod of 10 ± 1 hours.

13 **b. Critical depth hypothesis**

14 Next, we test whether the start of the Nordic Seas blooms is consistent with the critical
15 depth hypothesis, i.e. the blooms begin when $\frac{1}{H} \langle \bar{\mu} \rangle \geq m$ before they are detected by the
16 fluorometers. In this interpretation, the coincidence of the emergence of the fluorescence signal
17 from noise and the photoperiod must be considered a statistical fluke. Since we cannot determine
18 the loss rates during part of the winter north of the Arctic Circle, we first conduct the analysis on
19 the two events that did not experiment the polar night. Then, assuming that the winter grazing
20 pressure north of the Arctic Circle is no larger than south of it (phytoplankton concentrations are
21 smaller and ML deeper), we test if the Nordic Seas blooms start according to the critical depth
22 hypothesis.

1 For the two blooms sampled south of the Arctic Circle, $\langle \bar{\mu} \rangle$ is estimated as explained in
2 section 4bi. The phytoplankton loss rates are computed as a residual between division and
3 accumulation rates as described in the section 4bii. The last two panels of Fig. 3 show the time
4 series of the daily averaged insolation and of $\frac{1}{H} \langle \bar{\mu} \rangle$ and \bar{m} for the float IMR7 from November
5 2014 to June 2015 (an equivalent figure for the float IMR8 is displayed in the supplementary
6 material Fig. S11.). The figure reveals that $\frac{1}{H} \langle \bar{\mu} \rangle$ primarily tracks the increase in insolation; both
7 increase monotonically by close to two orders of magnitude from January to April. The division
8 rates instead track changes in loss rates during fall and spring. The winter loss rates never drop
9 below 0.02-0.05 day⁻¹, hereinafter denoted as \bar{m}_{winter} , whereas $\frac{1}{H} \langle \bar{\mu} \rangle$ drops to extremely low
10 values of $\sim 5 \cdot 10^{-3}$ day⁻¹. A loss rate of within a range of 0.05 - 0.1 day⁻¹ is believed to describe
11 background non-grazing phytoplankton mortality rates (Behrenfeld et al., 2013; Dutkiewicz et
12 al., 2015; Evans and Parslow, 1985; Moore et al., 2002). Thus our estimate supports the
13 hypothesis that grazing was very weak in winter.

14 The bloom onset did not seem to track changes in ML depth. The onset was estimated as
15 the time when $[\text{Chl}]_{\text{ML}}$ or $\langle \text{Chl} \rangle$ first increased. For the float-year IMR7 2014-2015, the bloom
16 onset occurred during a rapid shoaling of the ML, resulting in an increase of $[\text{Chl}]_{\text{ML}}$ and a
17 decrease in $\langle \text{Chl} \rangle$ due to detrainment. For the float-year IMR8 2013-2014, the bloom onset
18 coincided with a rapid deepening of the ML, resulting in an increase of $\langle \text{Chl} \rangle$ and a decrease in
19 $[\text{Chl}]_{\text{ML}}$ due to dilution with fluid with no phytoplankton from below. Figs. 3e and S11e show
20 that $\frac{1}{H} \langle \bar{\mu} \rangle$ changed somewhat in response to these ML changes, but much less than is response to
21 the rapid increase in isolation. We conclude that the blooms south of the Arctic Circle most
22 likely started because of the increase in insolation, which allowed division rates to exceed losses.

1 This scenario is consistent with the critical depth hypothesis, but not with Sverdrup's assumption
2 that it is changes in the ML depth that are key.

3 The same analysis is repeated for the nine blooms sampled north of the Arctic Circle. The
4 analysis can start only after time t_E , because prior to that time [Chl *a*] measurements are
5 dominated by noise and we cannot estimate loss rates. The average loss rates at t_E across all nine
6 blooms was $0.05 \pm 0.04 \text{ day}^{-1}$. This value is consistent with the winter phytoplankton loss rates
7 range estimated south of the Arctic Circle. We are therefore confident to assume that loss rates in
8 winter were likely no larger than $\sim 0.05 \text{ day}^{-1}$. In order to test if the bloom onset was consistent
9 with the critical depth hypothesis, we next test whether $\frac{1}{H} \langle \bar{\mu} \rangle$ exceeded the upper bound for
10 \bar{m}_{winter} of 0.05 day^{-1} during Δt_{onset} .

11 Fig. 6a shows the time series of $\frac{1}{H} \langle \bar{\mu} \rangle$ with time axis shifted so that for each of the nine
12 years the origin is at t_E . In all years, $\frac{1}{H} \langle \bar{\mu} \rangle$ exceeded 0.05 day^{-1} within the month prior to $t = t_E$.
13 Moreover, as shown for the events sampled south of the Arctic Circle, $\frac{1}{H} \langle \bar{\mu} \rangle$ primarily tracked
14 the increase in insolation. Fig. 6b shows that the dramatic increase in $\frac{1}{H} \langle \bar{\mu} \rangle$ disappears, if the
15 seasonal increase in surface insolation is ignored – iPAR (0, t) was replaced with a periodic
16 repetition of the daily cycle of incoming surface insolation on March 1st at 70 °. Surprisingly,
17 even the deep MLs sampled by floats IMR2 and IMR3 had little impact in delaying the increase
18 in division rates driven by the surface insolation. One may however argue that the delay in t_E for
19 these two events is an artifact of [Chl *a*] remaining too low to be detected in the deep MLs.

20 Our data are thus consistent with the hypothesis that the Nordic Seas blooms start
21 according to the critical depth hypothesis. But the analysis falls short of proving that the

1 deepening of critical depth at the end of winter is the trigger of the bloom. Such a proof would
2 require accurate estimates of winter division and loss rates, which are simply impossible to
3 obtain with present technology. Moreover, fluorometers with lower noise threshold are needed to
4 document the first accumulation of chlorophyll in the Nordic Seas winter, when concentrations
5 are extremely low.

6 In conclusion, the bloom onset is consistent with the photoperiod hypothesis if the
7 chlorophyll started to accumulate when it was first detected by the fluorometer. However, it is
8 also possible that the bloom started earlier according to the critical depth hypothesis, if some
9 weak accumulation started earlier in the season at levels too low to be detected by fluorometers.
10 Our opinion is that the photoperiod hypothesis is more likely to be correct, because it does not
11 seem likely that the co-occurrence of a critical photoperiod of 10 ± 1 hours and the increase in
12 chlorophyll detected by the fluorometers is mere coincidence.

13

14 **6. Conclusion**

15 In the Nordic Seas, north of the Arctic Circle, insolation drops so dramatically in winter
16 that phytoplankton growth is impossible for days to weeks during polar nights. The goal of this
17 paper was to investigate how do phytoplankton populations survive such harsh winter conditions
18 and what triggers their resurgence in spring. Satellite data are hardly ever available at these
19 latitudes due to continuous cloud coverage. Instead, we used in-situ data of [Chl *a*] and CTD
20 from six bio-optical floats deployed in this region.

1 Not surprisingly, the Chl *a* concentrations dropped dramatically in winter, during polar
2 nights, to values lower than reported by floats south of the Arctic Circle. The values were so low
3 that they were below or at the noise threshold levels of the traditional fluorometers mounted on
4 the floats. After a few months, at the end of winter, the Chl *a* concentrations started increasing
5 very rapidly. We cannot definitively conclude that this increase marked the bloom onset, because
6 low Chl *a* accumulation could have started earlier in the season at levels below the fluorometers
7 detection levels. This uncertainty in the exact timing of the bloom onset implies that the float
8 data are consistent with two possible scenarios for the onset of blooms in the Nordic Seas: the
9 critical photoperiod hypothesis and the critical depth hypothesis.

10 In all years sampled by the floats, the increase in Chl *a* concentrations was detected when
11 the phytoplankton experienced a photoperiod of 10 ± 1 hours, i.e. when phytoplankton
12 experienced approximately 10 light hours in a day for the first time in the season. The critical
13 photoperiod was equal to a 10 hours daylength, when mixing was weak, but it corresponded to a
14 longer daylength, when mixing was strong and kept cells away from the well-lit surface. We
15 speculate that similarly to what has been documented in the coastal waters of the Nordic Seas,
16 phytoplankton enters in resting stages during polar night in order to minimize energy
17 expenditure. Unlike in coastal waters, the resting stage cannot be in the form of spores or cysts
18 that are too dense to float in the open ocean. Rather the resting stage must be in the form of
19 vegetative cells whose density is closer to that of the water and can remain re-suspended for long
20 periods of time (D'Asaro, 2008).

21 The chlorophyll concentrations dropped below the noise level of our fluorometers in
22 winter. It is possible that some weak biomass accumulation started early in the season, but at
23 concentrations too weak to be detected by the fluorometers. We thus tested whether conditions

1 were favorable for bloom initiation prior to the first chlorophyll increase measured by the
2 fluorometers. In particular we investigated whether phytoplankton division rates were likely to
3 have exceeded losses in the weeks between the end of the polar night and the first chlorophyll
4 increase, consistent with the more commonly accepted critical depth hypothesis. The float data
5 suggest that changes in the ML depth and heat losses had little impact on the division rates in the
6 Nordic Seas at the end of winter. Furthermore, the winter grazing rates were likely lower than
7 non-grazing mortality due to parasitism and viral lysis. Thus dilution of grazers did not appear to
8 have much an effect on the increase in phytoplankton populations. Insolation instead increased
9 very rapidly at the end of winter north of the Arctic Circle and may have driven an increase in
10 division rates large enough to overcome losses. According to our analysis the increased
11 insolation ought to have triggered the blooms before they were detected by the fluorometers. A
12 possible scenario, given that the fluorometer signals were dominated by noise in winter. But a
13 scenario we cannot test with our data.

14 We tend to favor the first scenario, because it is hard to believe that the co-occurrence of
15 the bloom onset with a specific photoperiod is pure coincidence. However, the photoperiod
16 hypothesis implies that all species within the population start dividing at a critical photoperiod.
17 To our knowledge, such behavior has never been explored. Therefore, future work will have to
18 investigate if all species within the population have a critical photoperiod for initiating cell
19 division to assess whether the photoperiod hypothesis is tenable

20 Theory and models of high latitude ocean blooms do not consider the possibility that
21 phytoplankton enter and exit from resting stages in response to changes in photoperiod. This
22 omission can potentially impact the whole representation of these ecosystems, because the
23 timing of bloom initiation has been shown to impact on all the trophic levels affecting, for

1 example, the survival of larval fish (Platt et al., 2003) and the hatching time of shrimp eggs
2 (Koeller et al., 2009). Furthermore, an accurate representation of the timing and evolution of the
3 bloom is crucial to represent the ocean ecosystem response to climate change and its impact on
4 the ocean carbon budget.

1
2
3
4
5
6
7
8
9
10
11
12
13
14
15
16
17
18
19
20
21

7. Appendix: Calculation of the photoperiod

The photoperiod is the time spent by a cell in the euphotic layer within one day. In the open ocean this time depends on the length of daytime, the thickness of the euphotic layer and the trajectories of a cell in the turbulent mixed layer. The estimation of the euphotic layer depth and the calculation of the cell trajectories are discussed below.

a) Calculation of the euphotic layer depth

The daily-averaged euphotic layer depth (H_{eu}), defined as depth below which the light level is too low to support photosynthesis, was calculated by averaging Eq. (5) over the length of the day. The euphotic layer depths estimated was in the range of 150 to 170 m with a mean value of 165 ± 5 m. In the following calculations, the mean value across all nine years are used as representative of a lower bound on the winter euphotic layer depth.

b) Calculation of the turbulent velocity in a convective mixed layer

Mixed layer turbulence can be driven by heat fluxes, freshwater fluxes or winds. In the North Atlantic, upper ocean turbulence is generated by the surface heat with minor contributions from freshwater fluxes and winds (Ferrari et al., 2014). Hence the analysis will focus on mixed layers forced by heat fluxes.

The root mean square vertical velocity in a mixed layer forced by thermal convection in a nonrotating environment follows the following scaling verified by numerous laboratory

1 experiments (Deardorff and Willis, 1985; Fernando et al., 1991), and numerical simulations
2 (Deardorf, 1972; Molemaker and Dijkstra, 1997),

$$3 \quad w_{\text{rms}} = A|B_0 H|^{1/3}, \quad (\text{A2})$$

4 where H is the mixing layer depth, i.e the depth to which mixing penetrates (or equivalently the
5 mixed layer depth, since mixing typically extends to the whole mixed layer during winter
6 convection). B_0 is the surface buoyancy flux, and A is an order one coefficient of proportionality.
7 When the surface density is only affected by temperatures changes, B_0 can be related to the
8 surface heat flux $B_0 = \alpha g Q_0 / (c_p \rho_0)$, where c_p is the heat capacity, α is the thermal expansion
9 coefficient, ρ_0 is the water density, and g is the gravitational acceleration.

10 D'Asaro and collaborators (D'Asaro, 2001, 2008; Steffen and D'Asaro, 2002; Tseng and
11 D'Asaro, 2004) using trajectories of Lagrangian floats have shown that the scaling applies also
12 to winter convection in the real ocean. In particular Steffen and D'Asaro (2002) found that Eq.
13 (A2) applies to convection in the North Atlantic with a coefficient A in the range 0.3-0.6. In the
14 following calculations we will set $A = 0.45 \pm 0.15$.

15

16 **c) Calculation of the cell residence time in the euphotic layer during a** 17 **convection event**

18 Armed with estimates of the euphotic layer depth and the magnitude of the turbulent
19 velocity, we can now estimate the fraction of time that a particle spends in the euphotic layer
20 during convection. We idealize the looping trajectories in turbulent convective cells as periodic
21 oscillations between the ocean surface and the mixing layer depth H,

$$22 \quad z(t) = H/2 [\cos(\Omega t) - 1], \quad (\text{A3})$$

1 where $T=2\pi/\Omega$ is the period of the oscillations. The vertical velocity of the particles is therefore
 2 given by

$$3 \quad w = dz/dt = -H \Omega/2 \sin (\Omega t). \quad (A4)$$

4 Averaging w^2 over a period, we obtain the root-mean-square velocity, $w_{\text{rms}} = \sqrt{2}/2 H \Omega$. This
 5 expression, together with the scaling law for w_{rms} , in Eq. (A2), gives a scaling law for the
 6 frequency Ω and the period of the oscillations in the mixed layer,

$$7 \quad \Omega = 2\sqrt{2} A|B_0 H|^{1/3} / H, \quad \text{and} \quad T = (\pi H) / (\sqrt{2}A|B_0 H|^{1/3}). \quad (A5)$$

8 To assess the skill of the scaling for T , we compared the prediction of T from Eq. (A5)
 9 with two estimates of the overturning timescale from Lagrangian floats deployed in the North
 10 Atlantic (Steffen and D'Asaro, 2002). The results are reported in Table C1. Eq. (A5) predicts
 11 overturning timescales of 1.5 ± 0.6 and 1.3 ± 0.5 days using the observed mixed layer depths and
 12 heat fluxes in good agreement with float based estimates of 1.2 and 1.6 days respectively.

13 The residency time of particles in the euphotic layer is now easily computed as the time a
 14 trajectory spends between the surface and the euphotic layer depth H_{eu} . Assuming that the
 15 overturning timescale T is longer than the length of daytime, then the particles will visit the
 16 euphotic layer only once per day for a period of time given by,

$$17 \quad T_{\text{eu}} = (H \arccos (1-2H_{\text{eu}}/H)) / (\sqrt{2} A|B_0 H|^{1/3}) . \quad (A6)$$

18 Figure B1 plots the residency time T_{eu} as a function of mixed layer depth and heat flux,
 19 for the typical euphotic depth during winter in the region considered, $H_{\text{eu}} = 165$ m. For MLDs
 20 close to the euphotic depth, the particle speed are slow enough that cells in the euphotic layer
 21 experience light most of the daytime. For MLDs deeper than 200 m, the time spent in the
 22 euphotic layer decreases with increasing heat flux and is very weakly dependent on the mixing
 23 layer depth. One can understand this dependence taking the limit of Eq. (A6) for $H_{\text{eu}}/H \ll 1$,

1
$$T_{eu} \sim 2/A\sqrt{2} H_{eu}^{1/2} H^{1/6} |B_0|^{-1/3}. \quad (A7)$$

2 The increase in w_{rms} for increasing H is offset by the decrease in speed close to the surface
3 resulting into a weak dependence on H.

4 The residency time of phytoplankton cells in the upper 165 m at the onset of all 9 blooms
5 is shown in Fig. B1. The surface heat flux was estimated as the median value of Q_0 in the time
6 interval between the last profile before t_E and the profile at t_E . Its uncertainty was defined as the
7 semi-interquartile range of Q_0 in the same time interval. For most blooms H was estimated as the
8 median ML depth between the last profile before t_E and the profile at t_E . The uncertainty in H
9 was set equal to the difference in ML depth between the last profile before t_E and the profile at t_E .
10 For the blooms IMR3 2010-2011 and IMR3 2011-2012, the [Chl *a*] was observed to increase in a
11 layer shallower than the density-based estimate of the MLD. The MLD is a poor estimator of the
12 mixing layer depth as it may miss any slight restratification near the surface and it may also
13 record past deeper mixing events. For these two blooms, it is therefore more appropriate to
14 estimate H as the depth of the layer where we observed an increase of [Chl *a*], which likely
15 tracks the region where mixing is active.

16

17 Figure B1 shows that H was shallower than H_{eu} at t_E of four of the blooms and therefore
18 the cells remained in the euphotic layer for the whole length of daytime. At t_E of the remaining
19 three, the cell residency time in the upper 165 m is estimated to have been longer than or equal to
20 9 hours.

21

22 **d) Calculation of the photoperiod**

1 The photoperiod is the number of hours for which phytoplankton cells are exposed to
2 light during the day, i.e, the daily time spent in the euphotic layer. If the residency time T_{eu} is
3 longer than the daylength or the mixing layer is shallower than the euphotic depth, then the
4 photoperiod for cells in the euphotic layer is equal to the daylength; otherwise the photoperiod is
5 shorter and equal to T_{eu} . The Table C2 summarizes the daylength, H , Q_0 and our estimate of T_{eu}
6 at each bloom onset.

7 In seven blooms, t_E occurred when the daylength was between 9 and 11 hours (Table C2).
8 During that period, the surface heat losses remained smaller than 200 W m^{-2} . For heat fluxes of
9 this magnitude, cells spent more than 9 hours in the upper 165 m as per Fig. B1, while the
10 daylength was shorter. Hence the photoperiod was equal to the daylength and was between 9 and
11 11 hours on the day of t_E . The two hour spread in photoperiod values most likely stems from the
12 10 day sampling of the floats, which is equivalent to a one hour change in daylength at the
13 latitudes sampled by the floats. We conclude that the critical photoperiod when phytoplankton
14 cells germinate is 10 hours with an uncertainty of one hour for these seven bloom events.

15 In the remaining two float years, t_E occurred when the daylength was around 14 hours
16 (Table C2). The two floats were within 30 km of each other at bloom onset, so the two events are
17 not really independent. In both cases, the heat losses were constantly above 200 W m^{-2} as the
18 daylength increased from 9 to 14 hours, as can be seen in Fig. 4a looking at the 40 days prior to
19 bloom onset. According to Fig. B1, such a strong heat flux generated enough mixing to prevent
20 cells from experiencing more than 8 hours of light. Thus, from the point of view of the cells, the
21 photoperiod did not exceed 10 hours until the surface heat fluxes decreased at the end of March
22 and the daylength was already 14 hours. We conclude that the bloom onset is consistent with a
23 10-hour critical photoperiod for these two blooms as well.

1
2
3
4
5
6
7
8
9
10
11
12
13
14
15
16
17
18
19
20
21
22
23
24
25
26

8. Acknowledgements.

Alexandre Mignot and Raffaele Ferrari acknowledge NSF support through award OCE-1155205. This paper represents a contribution to the E-AIMS projects, which is funded by the European Research Council (grant agreement no. 312642). We thank the crew of the various cruises who deployed the Bio-optical floats used in the present study. We also acknowledge many insightful conversations with Herve Claustre, Glenn Flierl, Emmanuel Boss and Mike Behrenfeld.

9. References:

Antoine, D. and Morel, A.: Oceanic primary production: 1. Adaptation of a spectral light-photosynthesis model in view of application to satellite chlorophyll observations, *Glob. Biogeochem. Cycles*, 10(1), 43–55, doi:10.1029/95GB02831, 1996.

Behrenfeld, M. J.: Abandoning Sverdrup’s Critical Depth Hypothesis on phytoplankton blooms, *Ecology*, 91(4), 977–989, doi:10.1890/09-1207.1, 2010.

Behrenfeld, M. J.: Climate-mediated dance of the plankton, *Nat. Clim Change*, 4(10), 880–887, 2014.

Behrenfeld, M. J., Doney, S. C., Lima, I., Boss, E. S. and Siegel, D. A.: Annual cycles of ecological disturbance and recovery underlying the subarctic Atlantic spring plankton bloom, *Glob. Biogeochem. Cycles*, 27(2), 526–540, doi:10.1002/gbc.20050, 2013.

Boss, E., Swift, D., Taylor, L., Brickley, P., Zaneveld, R., Riser, S., Perry, M. J. and Strutton, P. G.: Observations of pigment and particle distributions in the western North Atlantic from an autonomous float and ocean color satellite, *Limnol. Oceanogr.*, 53(5), 2112–2122, doi:10.4319/lo.2008.53.5_part_2.2112, 2008.

Brainerd, K. and Gregg, M.: Surface Mixed and Mixing Layer Depths, *Deep-Sea Res. Part - Oceanogr. Res. Pap.*, 42(9), 1521–1543, doi:10.1016/0967-0637(95)00068-H, 1995.

- 1 Budyko, M. I., Donehoo, I. A., Akademiia nauk SSSR and Mezhdovedomstvennyiĭ geofizicheskiĭ
2 komitet: Guide to the atlas of the heat balance of the earth: (atlas teplovogo balansa zemnogo
3 shara), U.S. Dept. of Commerce, Weather Bureau, Washington, D.C., 1964.
- 4 D'Asaro, E. A.: Turbulent vertical kinetic energy in the ocean mixed layer, *J. Phys. Oceanogr.*,
5 31(12), 3530–3537, doi:10.1175/1520-0485(2002)031<3530:TVKEIT>2.0.CO;2, 2001.
- 6 D'Asaro, E. A.: Convection and the seeding of the North Atlantic bloom, *J. Mar. Syst.*, 69(3-4),
7 233–237, doi:10.1016/j.jmarsys.2005.08.005, 2008.
- 8 Deardorff, J. and Willis, G.: Further Results from a Laboratory Model of the Convective
9 Planetary Boundary-Layer, *Bound.-Layer Meteorol.*, 32(3), 205–236, doi:10.1007/BF00121880,
10 1985.
- 11 Deardorf, J.: Numerical Investigation of Neutral and Unstable Planetary Boundary-Layers, *J.*
12 *Atmospheric Sci.*, 29(1), 91–&, doi:10.1175/1520-0469(1972)029<0091:NIONAU>2.0.CO;2,
13 1972.
- 14 Dee, D. P., Uppala, S. M., Simmons, A. J., Berrisford, P., Poli, P., Kobayashi, S., Andrae, U.,
15 Balmaseda, M. A., Balsamo, G., Bauer, P., Bechtold, P., Beljaars, A. C. M., van de Berg, L.,
16 Bidlot, J., Bormann, N., Delsol, C., Dragani, R., Fuentes, M., Geer, A. J., Haimberger, L., Healy,
17 S. B., Hersbach, H., Holm, E. V., Isaksen, L., Kallberg, P., Koehler, M., Matricardi, M.,
18 McNally, A. P., Monge-Sanz, B. M., Morcrette, J.-J., Park, B.-K., Peubey, C., de Rosnay, P.,
19 Tavolato, C., Thepaut, J.-N. and Vitart, F.: The ERA-Interim reanalysis: configuration and
20 performance of the data assimilation system, *Q. J. R. Meteorol. Soc.*, 137(656), 553–597,
21 doi:10.1002/qj.828, 2011.
- 22 Degerlund, M. and Eilertsen, H. C.: Main Species Characteristics of Phytoplankton Spring
23 Blooms in NE Atlantic and Arctic Waters (68-80A degrees N), *Estuaries Coasts*, 33(2), 242–269,
24 doi:10.1007/s12237-009-9167-7, 2010.
- 25 Dutkiewicz, S., Hickman, A. E., Jahn, O., Gregg, W. W., Mouw, C. B. and Follows, M. J.:
26 Capturing optically important constituents and properties in a marine biogeochemical and
27 ecosystem model, *Biogeosciences*, 12(14), 4447–4481, doi:10.5194/bg-12-4447-2015, 2015.
- 28 Eilertsen, H. and Wyatt, T.: Phytoplankton models and life history strategies, *South Afr. J. Mar.*
29 *Sci.*, 22(1), 323–338, 2000.
- 30 Eilertsen, H., Sandberg, S. and Tollefsen, H.: Photoperiodic Control of Diatom Spore Growth - a
31 Theory to Explain the Onset of Phytoplankton Blooms, *Mar. Ecol. Prog. Ser.*, 116(1-3), 303–
32 307, doi:10.3354/meps116303, 1995.
- 33 Evans, G. T. and Parslow, J. S.: A Model of Annual Plankton Cycles, *Biol. Oceanogr.*, 3(3),
34 327–347, doi:10.1080/01965581.1985.10749478, 1985.
- 35 Fernando, H., Chen, R. and Boyer, D.: Effects of Rotation on Convective Turbulence, *J. Fluid*
36 *Mech.*, 228, 513–547, doi:10.1017/S002211209100280X, 1991.

- 1 Ferrari, R., Merrifield, S. T. and Taylor, J. R.: Shutdown of convection triggers increase of
2 surface chlorophyll, *J. Mar. Syst.*, doi:10.1016/j.jmarsys.2014.02.009, 2014.
- 3 Forsythe, W., Rykiel, E., Stahl, R., Wu, H. and Schoolfield, R.: A Model Comparison for
4 Daylength as a Function of Latitude and Day of Year, *Ecol. Model.*, 80(1), 87–95,
5 doi:10.1016/0304-3800(94)00034-F, 1995.
- 6 Geider, R., Osborne, B. and Raven, J.: Growth, Photosynthesis and Maintenance Metabolic Cost
7 in the Diatom *Phaeodactylum-Tricornutum* at Very Low Light Levels, *J. Phycol.*, 22(1), 39–48,
8 doi:10.1111/j.1529-8817.1986.tb02513.x, 1986.
- 9 Gran, H. H. and Braarud, T.: A Quantitative Study of the Phytoplankton in the Bay of Fundy and
10 the Gulf of Maine (including Observations on Hydrography, Chemistry and Turbidity), *J. Biol.*
11 *Board Can.*, 1(5), 279–467, doi:10.1139/f35-012, 1935.
- 12 Gregg, W. and Carder, K.: A Simple Spectral Solar Irradiance Model for Cloudless Maritime
13 Atmospheres, *Limnol. Oceanogr.*, 35(8), 1657–1675, 1990.
- 14 Hamner, K. C.: Interrelation of Light and Darkness in Photoperiodic Induction, *Bot. Gaz.*,
15 101(3), 658–687, 1940.
- 16 Hamner, K. C. and Bonner, J.: Photoperiodism in Relation to Hormones as Factors in Floral
17 Initiation and Development, *Bot. Gaz.*, 100(2), 388–431, 1938.
- 18 Kara, A. B., Rochford, P. A. and Hurlburt, H. E.: An optimal definition for ocean mixed layer
19 depth, *J. Geophys. Res.-Oceans*, 105(C7), 16803–16821, doi:10.1029/2000JC900072, 2000.
- 20 Kara, A. B., Rochford, P. A. and Hurlburt, H. E.: Mixed layer depth variability over the global
21 ocean, *J. Geophys. Res.-Oceans*, 108(C3), doi:10.1029/2000JC000736, 2003.
- 22 Koeller, P., Fuentes-Yaco, C., Platt, T., Sathyendranath, S., Richards, A., Ouellet, P., Orr, D.,
23 Skuladottir, U., Wieland, K., Savard, L. and Aschan, M.: Basin-Scale Coherence in Phenology of
24 Shrimps and Phytoplankton in the North Atlantic Ocean, *Science*, 324(5928), 791–793,
25 doi:10.1126/science.1170987, 2009.
- 26 McMinn, A. and Martin, A.: Dark survival in a warming world, *Proc. Biol. Sci.*, 280(1755),
27 20122909, doi:10.1098/rspb.2012.2909, 2013.
- 28 Molemaker, M. J. and Dijkstra, H. A.: The formation and evolution of a diffusive interface, *J.*
29 *Fluid Mech.*, 331, 199–229, doi:10.1017/S0022112096003862, 1997.
- 30 Moore, J. K., Doney, S. C., Kleypas, J. A., Glover, D. M. and Fung, I. Y.: An intermediate
31 complexity marine ecosystem model for the global domain, *Deep-Sea Res. Part II-Top. Stud.*
32 *Oceanogr.*, 49(1-3), 403–462, doi:10.1016/S0967-0645(01)00108-4, 2002.
- 33 Morel, A., Huot, Y., Gentili, B., Werdell, P. J., Hooker, S. B. and Franz, B. A.: Examining the
34 consistency of products derived from various ocean color sensors in open ocean (Case 1) waters

1 in the perspective of a multi-sensor approach, *Remote Sens. Environ.*, 111(1), 69–88,
2 doi:10.1016/j.rse.2007.03.012, 2007.

3 Platt, T., Fuentes-Yaco, C. and Frank, K. T.: Spring algal bloom and larval fish survival, *Nature*,
4 423(6938), 398–399, doi:10.1038/423398b, 2003.

5 R Development Core Team: R Development Core Team (2016). *R: A language and environment*
6 *for statistical computing*. R Foundation for Statistical Computing, Vienna, Austria. ISBN 3-
7 900051-07-0, URL <http://www.R-project.org>, 2016.

8 Riley, G.: Factors Controlling Phytoplankton Populations on Georges Bank, *J. Mar. Res.*, 6(1),
9 54–73, 1946.

10 Skjelvan, I., Olsen, A., Anderson, L. G., Bellerby, R. G. J., Falck, E., Kasajima, Y., Kivimäe, C.,
11 Omar, A., Rey, F., Olsson, K. A., Johannessen, T. and Heinze, C.: A review of the inorganic
12 carbon cycle of the Nordic Seas and Barents Sea, in *Geophysical Monograph Series*, vol. 158,
13 edited by H. Drange, T. Dokken, T. Furevik, R. Gerdes, and W. Berger, pp. 157–175, American
14 Geophysical Union, Washington, D. C. [online] Available from:
15 <http://www.agu.org/books/gm/v158/158GM11/158GM11.shtml> (Accessed 25 April 2014), 2005.

16 Smith, R. and Baker, K.: Optical-Properties of the Clearest Natural-Waters (200-800 Nm), *Appl.*
17 *Opt.*, 20(2), 177–184, doi:10.1364/AO.20.000177, 1981.

18 Steffen, E. L. and D’Asaro, E. A.: Deep convection in the Labrador Sea as observed by
19 Lagrangian floats, *J. Phys. Oceanogr.*, 32(2), 475–492, doi:10.1175/1520-
20 0485(2002)032<0475:DCITLS>2.0.CO;2, 2002.

21 Sverdrup, H. U.: On Conditions for the Vernal Blooming of Phytoplankton, *J. Cons.*, 18(3), 287–
22 295, doi:10.1093/icesjms/18.3.287, 1953.

23 Takahashi, T., Sutherland, S. C., Sweeney, C., Poisson, A., Metzl, N., Tilbrook, B., Bates, N.,
24 Wanninkhof, R., Feely, R. A., Sabine, C., Olafsson, J. and Nojiri, Y.: Global sea-air CO₂ flux
25 based on climatological surface ocean pCO₂, and seasonal biological and temperature effects,
26 *Deep-Sea Res. Part II-Top. Stud. Oceanogr.*, 49(9-10), 1601–1622, doi:10.1016/S0967-
27 0645(02)00003-6, 2002.

28 Tseng, R. S. and D’Asaro, E. A.: Measurements of turbulent vertical kinetic energy in the ocean
29 mixed layer from Lagrangian floats, *J. Phys. Oceanogr.*, 34(9), 1984–1990, doi:10.1175/1520-
30 0485(2004)034<1984:MOTVKE>2.0.CO;2, 2004.

31 Westberry, T., Behrenfeld, M. J., Siegel, D. A. and Boss, E.: Carbon-based primary productivity
32 modeling with vertically resolved photoacclimation, *Glob. Biogeochem. Cycles*, 22(2), GB2024,
33 doi:10.1029/2007GB003078, 2008.

34 Wong, A., Keeley, R., Carval, T. and the Argo Data Management Team: Argo quality control
35 manual. Technical report, Argo Data Management team., 2010.

36

1

2 **Table 1.** Relevant Information concerning the 8 bio-optical profiling floats used in this study.

<i>Float</i>	<i>wmo number</i>	<i>Deployment location</i>	<i>Deployment Date</i>	<i>Sensor failure date</i>
IMR1	6900796	0.25°W, 67.68°N	30 May 2010	Optical sensors: 31 Oct 2012 CTD: 19 Jan 2013
IMR2	6900798	2.43°E, 69.09°N	02 Jul 2010	Optical sensors: 01 Nov 2012 CTD is still operational
IMR3	6900799	6.01°E, 70.03°N	06 Nov 2010	Optical sensors: 31 Oct 2012 CTD: 20 Sept 2013
IMR4	6902545	7.54°E, 69.27°N	23 Jan 2014	ongoing
IMR5	6902549	1.40°E, 72.57°N	29 Jul 2014	ongoing
IMR6	6902550	5.90°E, 70.78°N	04 Aug 2014	ongoing
IMR7	6902544	0.04°E, 64.66°N	16 Nov 2013	ongoing
IMR8	6902548	4.70°W, 68.58°N	21 Jul 2014	ongoing

3

4

1 **Table 2.** Fluorometer scale factors provided by the manufacturer, number of MODIS match-
 2 ups, regression slopes determined by a regression through the origin and correlation coefficients
 3 between the float fluorescence (minus the dark counts) and MODIS [Chl *a*] estimates.

<i>Float</i>	<i>Manufacturer scale factor (mg count⁻¹)</i>	<i>Number of MODIS matchups</i>	<i>Regression slope (mg m⁻³ count⁻¹)</i>	<i>Correlation coefficient</i>
IMR1	0.0072	82	0.0051	0.61
IMR2	0.0072	69	0.0034	0.69
IMR3	0.0074	62	0.0049	0.63
IMR4	0.0073	36	0.0026	0.44
IMR5	0.0072	42	0.0020	0.81
IMR6	0.0072	42	0.0013	0.63
IMR7	0.0073	32	0.0018	0.49
IMR8	0.0072	46	0.0024	0.53

4

5

1

2 **Table 3.** Time of “emergence from noise” (t_E) in year day, and latitude at t_E . The events have
3 been sorted in increasing day of the year from top to bottom.

<i>Bloom</i>	t_E	<i>Latitude</i>
IMR1 2011-2012	59	66.7
IMR1 2010-2011	62	68.5
IMR5 2014-2015	66	72.5
IMR3 2011-2012	69	69.9
IMR4 2014-2015	69	70.4
IMR2 2011-2012	70	70.5
IMR6 2014-2015	72	69.9
IMR3 2010-2011	95	69.4
IMR2 2010-2011	96	69.0

4

1 **Table C1.** Surface heat flux Q_0 , mixing layer depth H , and observed overturning time T_{obs} as
2 reported in (Steffen and D'Asaro, 2002). The corresponding predicted overturning time T_{mod} is
3 based on Eq. (A5) with the following parameters: $A = 0.45 \pm 15$, $c_p = 3986 \text{ J/Kg } ^\circ\text{C}$, $\alpha = 8.72 \times 10^{-4}$
4 $^\circ\text{C}^{-1}$, $g = 9.81 \text{ m}^2 \text{ s}^{-1}$, and $\rho_0 = 1027.764 \text{ kg m}^{-3}$ derived from the observed salinity and potential
5 temperature at the sea surface in (Steffen and D'Asaro, 2002). The T_{mod} uncertainties (ΔT_{mod})
6 are calculated as: $\Delta T_{\text{mod}} / T_{\text{mod}} = ((\Delta A / A) + (1/3) (\Delta H / H) + (1/3) (\Delta Q_0 / Q_0))$, with ΔA , ΔH ,
7 and ΔQ_0 being the uncertainties of A , H , and Q_0 .

8

	<i>1997</i>	<i>1998</i>
$Q_0 \text{ (W m}^{-2}\text{)}$	270 ± 40	150 ± 30
$H \text{ (m)}$	960 ± 30	620 ± 20
$T_{\text{obs}} \text{ (days)}$	1.2	1.6
$T_{\text{mod}} \text{ (days)}$	1.5 ± 0.6	1.3 ± 0.5

9

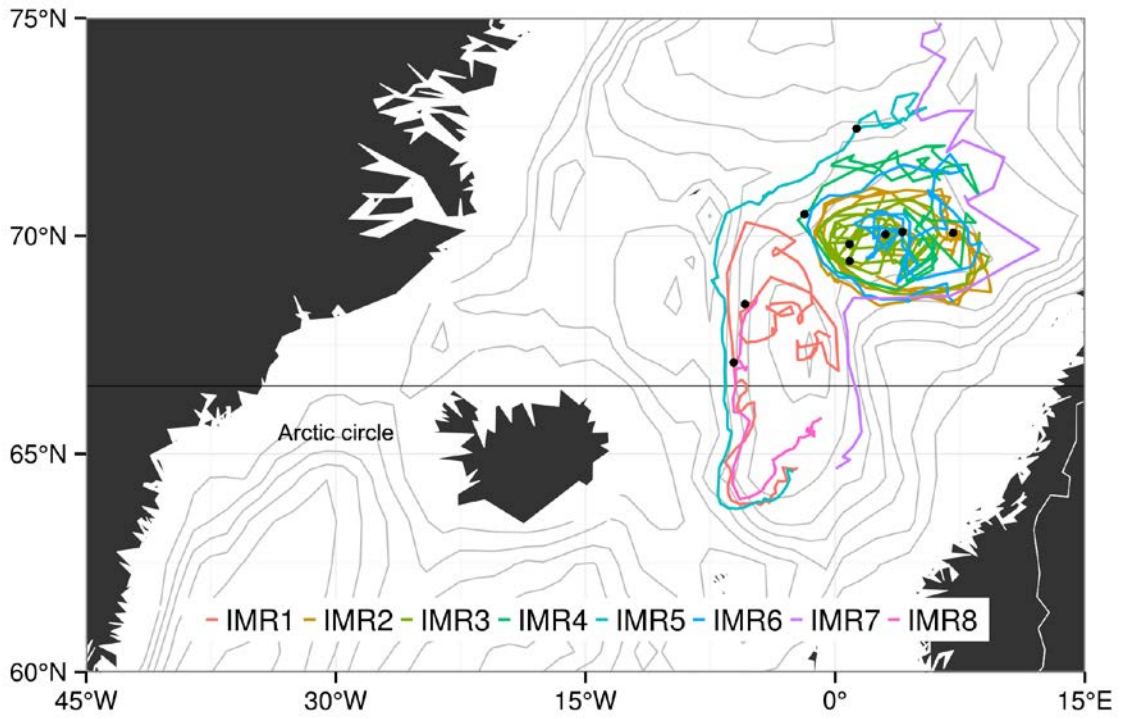
10

1 **Table C2.** Time of “emergence from noise” (t_E), daylength (hours), mixing layer depth (H), surface heat
2 flux Q_0 ($W\ m^{-2}$), the euphotic layer residency time (T_{eu}) and photoperiod at t_E . The daylength is the
3 estimated value at t_E . The estimates for Q_0 , H, and their uncertainty are discussed in the text. The
4 estimates of T_{eu} , based on Eq. A6, are only indicated if $H > H_{eu}=165$ m.

Bloom	t_E	Daylength (hrs)	H (m)	Q_0 ($W\ m^{-2}$)	T_{eu} (hrs)	Photoperiod (hrs)
IMR1a	2011-03-03	10	240 ± 50	-65 ± 70	12	10
IMR1b	2012-02-28	10	160 ± 20	-130 ± 60		10
IMR2a	2011-04-06	14	200 ± 170	-100 ± 100	11	11
IMR2b	2012-03-10	11	140 ± 30	-130 ± 20		11
IMR3a	2011-04-05	14	360 ± 310	-130 ± 120	10	10
IMR3a	2012-03-09	11	100 ± 10	-120 ± 20		11
IMR4	2015-03-10	11	320 ± 10	-150 ± 40	10	10
IMR5	2015-03-07	10	120 ± 10	-100 ± 30		10
IMR6	2015-03-13	11	330 ± 40	-170 ± 50	9	9

5

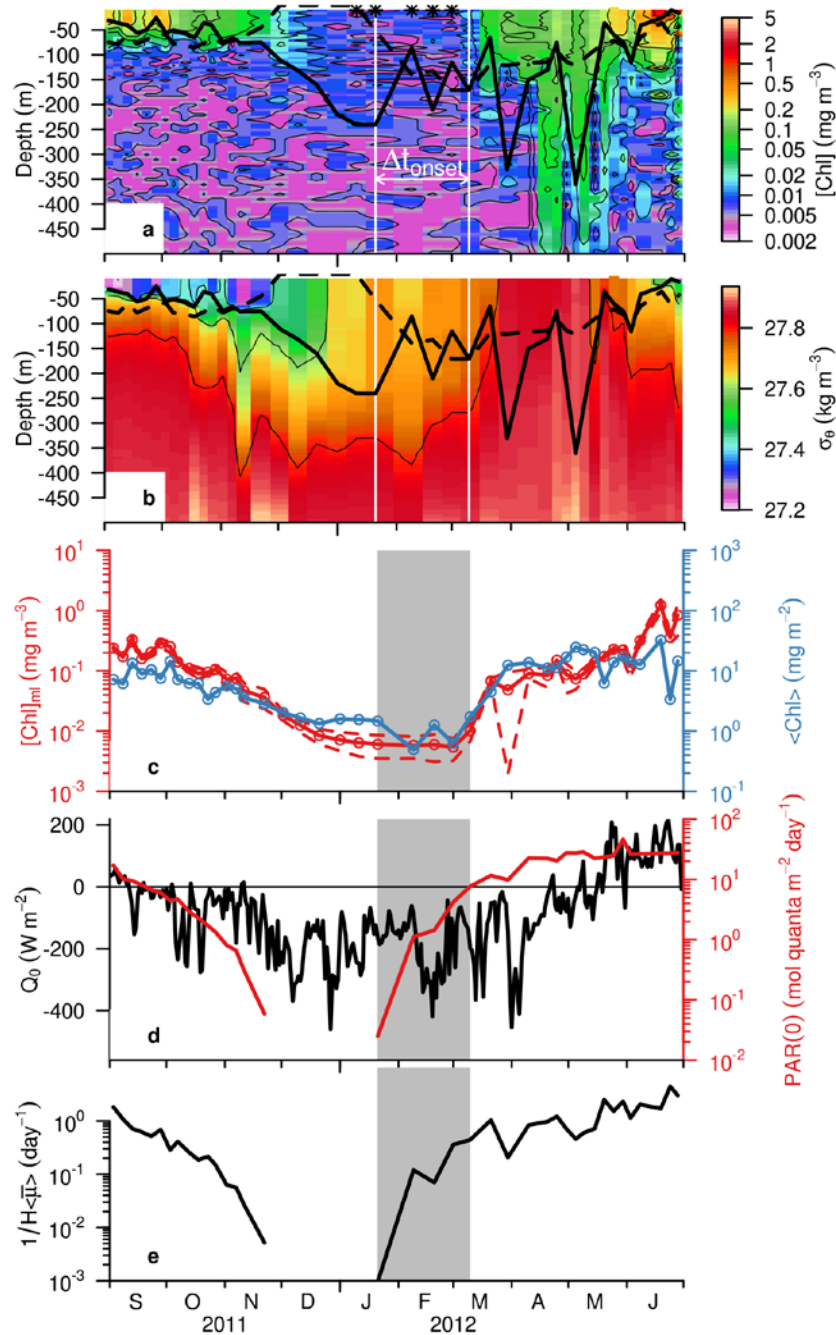
1



2

3 **Fig. 1.** Trajectory of the floats used in the study. The black symbols show the location of the
4 floats deployed North of the Arctic Circle (i.e., IMR1, IMR2, IMR3, IMR4, IMR5 and IMR6) at
5 t_E .

6



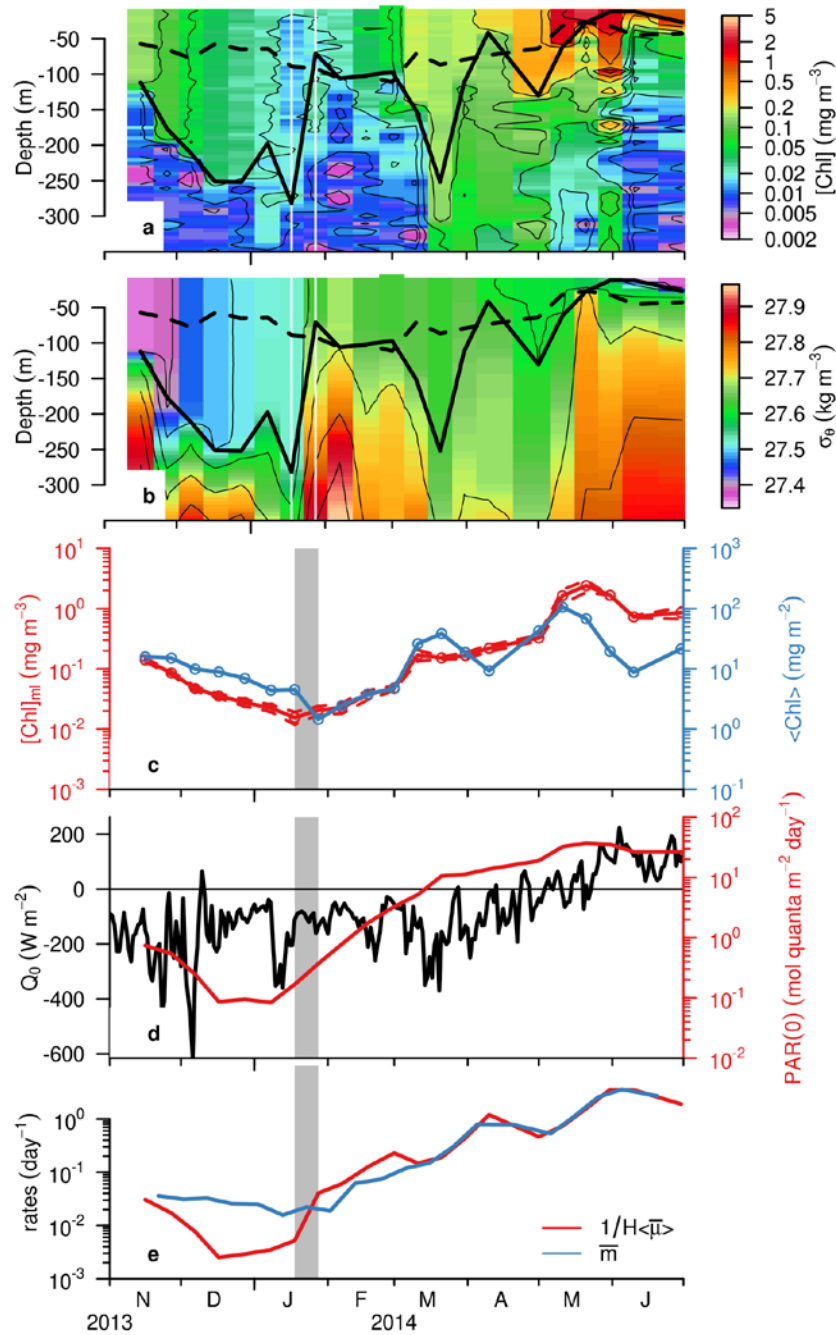
1

2 **Fig. 2.** Bloom observed by float IMR2 during the fall-spring 2011-2012. (a) Time evolution
 3 of the vertical distribution of [Chl *a*]. The asterisks symbolize the vertical profiles where the ML
 4 fluorescence values are not significantly different from the deep fluorescence values. (b) Time
 5 evolution of the vertical distribution of potential density σ_θ . The continuous and dashed black
 6 lines are the mixed layer, H, and euphotic layer depths, H_{eu}, respectively. (c) Time series of the
 7 vertical integral and the average concentration of [Chl *a*] in the ML (<Chl>, blue lines and

1 [Chl]_{ml}, red line). The dashed lines are the standard deviations around the average cycle of [Chl]_{ml}
2 .(d) Time series of the daily surface heat flux Q_0 (black line) and the daily surface PAR corrected
3 for cloud cover, PAR(0), (red line). (e) Time series of the division rate. The two white vertical
4 lines and the gray shading indicate Δt_{onset} ; period of time during which bloom onset is possible.
5 The second white vertical line indicates the sampling profile during which the ML fluorescence
6 become significantly different from the deep fluorescence values (i.e., emergence from signal to
7 noise, t_E).

8

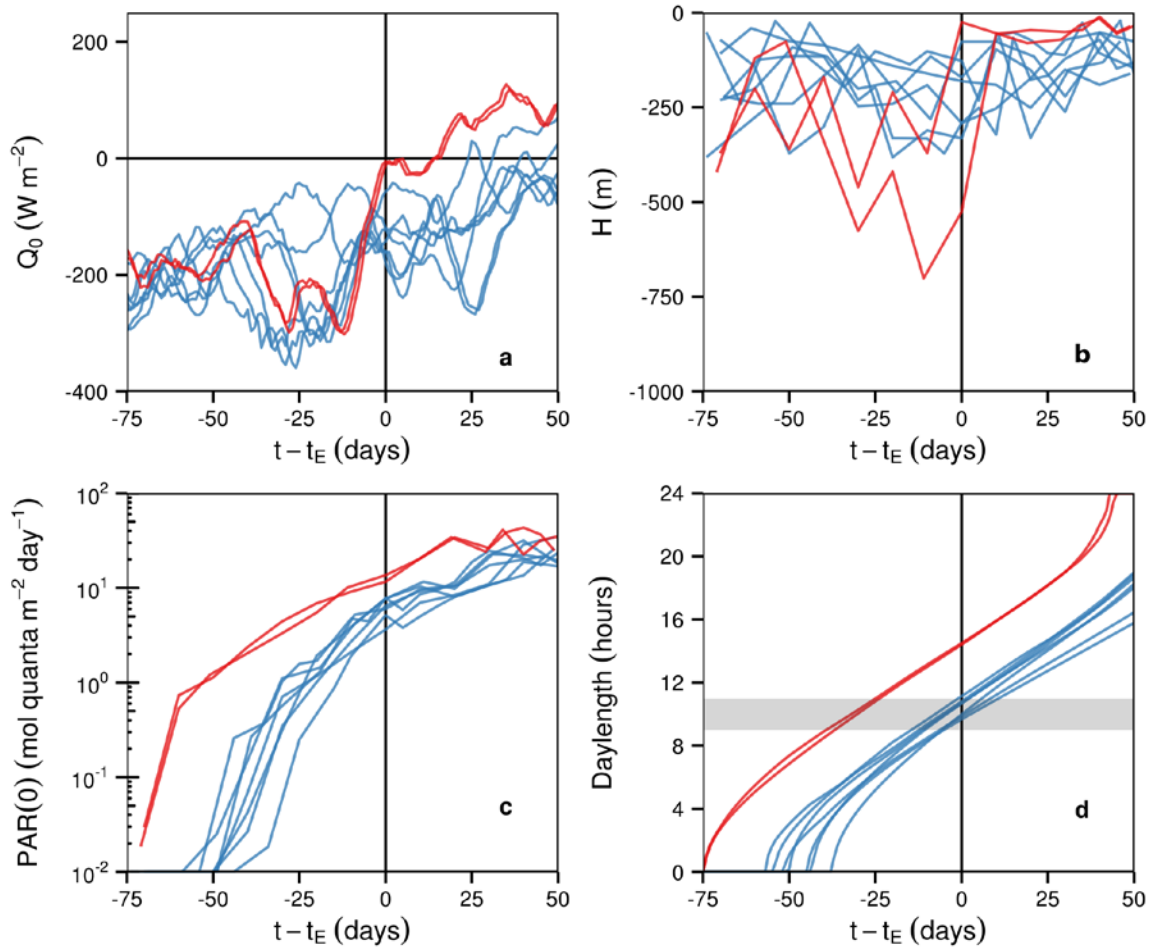
9



1

2 **Fig. 3.** Same as Fig. 2, but for the float IMR7 during the winter-spring 2013-2014. The two
 3 white vertical lines and the gray shading indicate the onset of the bloom. In panel (e), the
 4 continuous red and blue lines are the daily mixed layer averaged division rate ($1/H\langle\mu\rangle$) and the
 5 phytoplankton loss rates (m), respectively.

6



1

2

3

4

5

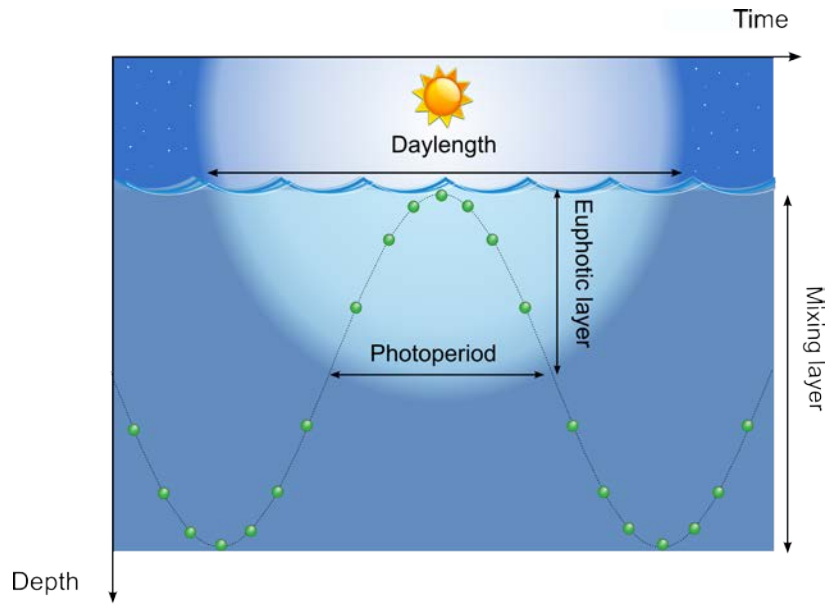
6

7

8

9

Fig.4. (a) Time series of surface heat flux (Q_0), (b) mixed layer depth (H), (c) the daily surface PAR corrected for cloud cover [$PAR(0)$], and (d) daylength relative to the time of “emergence from signal to noise” t_E for the eight bloom events observed by the floats. The blue lines represent the cases where the first accumulation of biomass was associated with negative sea surface heat fluxes. The red lines represent the cases where the first accumulation of biomass associated with the shutdown of the wintertime cooling. A 10-day moving average has been applied to Q_0 .



1

2

3

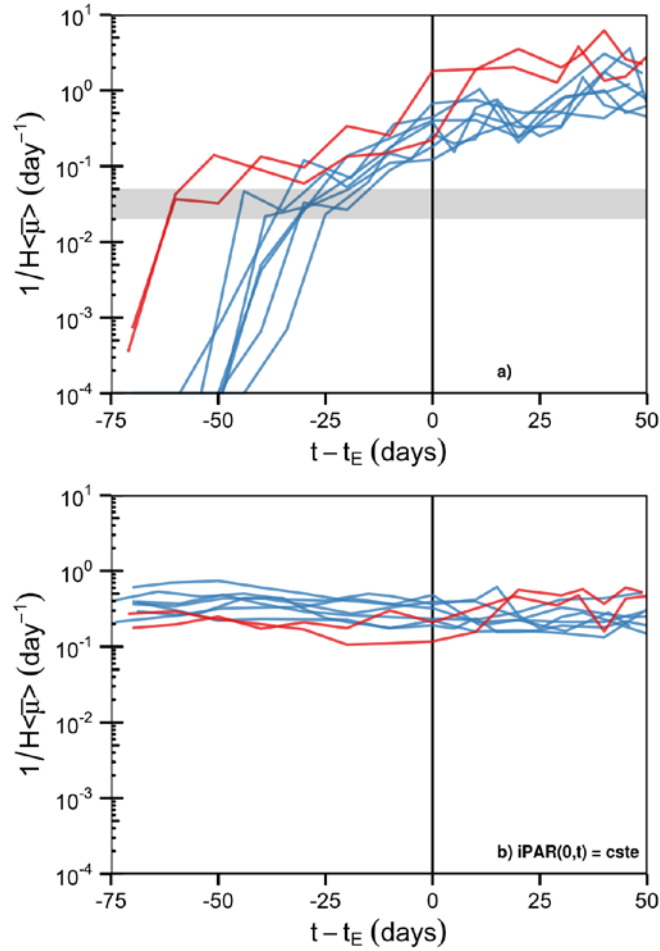
4

5

6

7

Fig. 5. Schematic of the trajectory of a phytoplankton cells in the mixing layer. The photoperiod is the time spent by the cell in the euphotic layer. In the open ocean, this time depends on the daylength, the depth of the euphotic layer, the strength and the vertical extent of the turbulence mixing the cells.



1

2

3

4

5

6

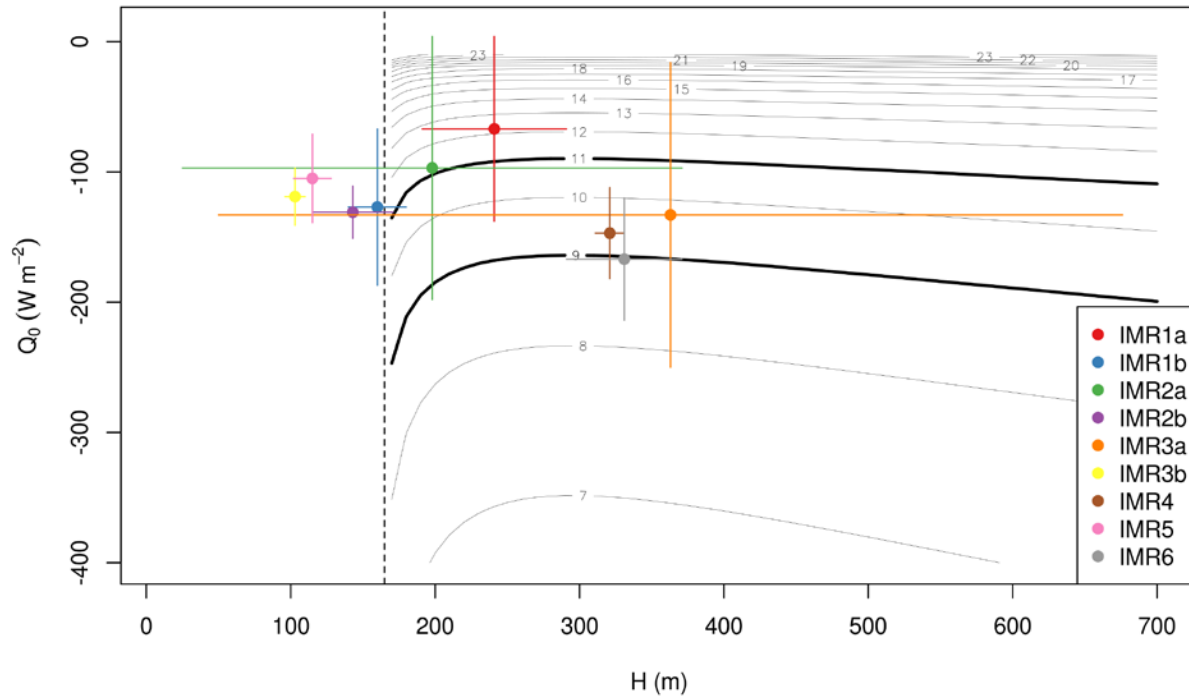
7

8

9

10

Fig. 6. Time series of the daily mixed layer-averaged phytoplankton division rate ($\frac{1}{H} \langle \bar{\mu} \rangle$) based on Eq. (14) relative to $t = t_E$ for the eight events observed by the floats. The blue lines represent an accumulation of biomass associated with negative sea surface heat fluxes. The red lines represent accumulation of biomass associated with the shutdown of the wintertime cooling. The horizontal gray shading represents the winter phytoplankton loss rates range, namely 0.02-0.05 day^{-1} . **(a)** Estimates based a clear sky model of incoming irradiance for the days and latitudes sampled by each float (Gregg and Carder, 1990). **(b)** Estimates based on the periodic repetition of the daily cycle of incoming surface insolation on March 1st at 70°N.



1
2 **Figure B1.** Residency time in the euphotic layer (T_{eu}) as a function of the mixing layer depth (H)
3 and the surface heat flux (Q_0) at the onset time of the bloom. The estimates are based on Eq. A6
4 with the following parameter values: $A=0.45$, $c_p=3984 \text{ J/Kg } ^\circ\text{C}$, $\alpha=1.22 \times 10^{-4} \text{ } ^\circ\text{C}^{-1}$, $g=9.81 \text{ m}^2 \text{ s}^{-1}$,
5 $\rho_0=1028 \text{ kg m}^{-3}$, (c_p , α and ρ_0 are the average values at the nine bloom onsets). The vertical
6 dashed line is the euphotic depth, $H_{eu} = 165\text{m}$. The estimates for Q_0 , H and their uncertainties are
7 discussed in the text.

8